Quantitative one-dimensional thermal-wave cavity measurements of fluid thermophysical properties through equivalence studies with three-dimensional geometries

Anna Matvienko and Andreas Mandelis[a)]
Center for Advanced Diffusion-Wave Technologies, Department of Mechanical and Industrial Engineering, University of Toronto, Toronto, Ontario M5S3G8, Canada

(Received 11 April 2006; accepted 13 May 2006; published online 22 June 2006)

The thermal-wave field in a photopyroelectric thermal-wave cavity was calculated with two theoretical approaches: a computationally straightforward, conventional, one-dimensional approach and a three-dimensional experimentally more realistic approach. The calculations show that the dimensionality of the thermal-wave field in the cavity depends on the lateral heat transfer boundary conditions and the relation between the beam size of the laser impinging on the thermal-wave generating metallic film and the diameter of the film itself. The theoretical calculations and the experimental data on the photopyroelectric signal in the cavity were compared. The study resulted in identifying ranges of heat transfer rates, beam sizes, and cavity radii for which accurate quantitative measurements of the thermal diffusivity of intracavity fluids can be made within the far simpler, but only approximate, one-dimensional approach conventionally adopted by users of thermal-wave cavities. It was shown that the major parameters affecting the dimensionality of thermal-wave cavities are the laser beam spot size and the Biot number of the medium comprising the sidewalls of the (cylindrical) cavity. © *2006 American Institute of Physics.*
[DOI: 10.1063/1.2212946]

I. INTRODUCTION

In recent years, photothermal techniques have been established as a powerful tool for the thermophysical characterization of materials. The common working principle of conventional photothermal techniques is based on the study of the periodic temperature distribution, i.e., thermal wave, produced in a given sample as a result of heating due to an intensity modulated pump laser source. The thermal wave inside a sample diffuses over a characteristic distance (thermal diffusion length[1]) depending on the modulation frequency and the thermal diffusivity of the sample. The resulting temperature distribution can be detected by various photothermal methods, most of which usually apply optical characterization, photothermal radiometry, or photopyroelectric detection.[2] The latter method can be applied to the high-resolution thermophysical characterization of solid,[3] liquid,[4–8] and gaseous[9–11] samples. In this case, a pyroelectric sensor [polyvinilidene fluoride (PVDF) films[3–5] or crystal disks of $LiTaO_3$ (Refs. 6 and 7)] attached to the sample is used as a detector of temperature oscillations. The first experimental device for the measurement in gaseous or liquid media, called thermal-wave resonator cavity (TWRC), was introduced in 1995.[9] In its original design, the cavity consisted of two walls: a very thin aluminum film exposed to a modulated laser beam, acting as a thermal-wave generator, and a pyroelectric film placed parallel to the thermal-source surface at a fixed distance, generating an electrical signal proportional to the detected temperature oscillations transmitted through the intracavity air gap. Since the introduction of TWRC, its various modifications have been increasingly used for accurate and precise thermophysical measurements. In addition to the original TWRC configuration, there are several modifications of the thermal-wave cavity reported in the literature, such as the reverse thermal-wave cavity configuration[6,7] and the interferometric thermal-wave cavity.[11] These experimental devices allowed measurements of thermal properties of gases and vapors,[9–11] water, alcohols and their mixtures,[4–7] oils, and food products.[8] It is possible to measure thermal properties of the intracavity media by analyzing the dependence of the measured photothermal signal on the modulation frequency[4,7,8] or the distance between the walls (cavity length).[5,6,9,10] Using conduction or conduction and radiation heat transfer, theoretical expressions for the fitting of thermal properties can be developed. These expressions are usually based on general photopyroelectric detection theory[12] and have a variety of modifications depending on the cavity configuration applied in the experiments. Almost always, the theoretical treatments adopt relatively simple one-dimensional thermal-wave field approaches.[3–13] There are configurations, however, where the actual distribution of the thermal-wave source and the TWRC length require a three-dimensional approach. To our best knowledge, there has been no attempt to develop three-dimensional theoretical models for the thermal wave field analysis in cavities. Without the comparison with the three-dimensional approach, the one-dimensional simplification may become unjustified, especially in cases of narrow laser beams and cavity lengths large compared with the thermal diffusion

[a)]Author to whom correspondence should be addressed; electronic mail: mandelis@mie.utoronto.ca

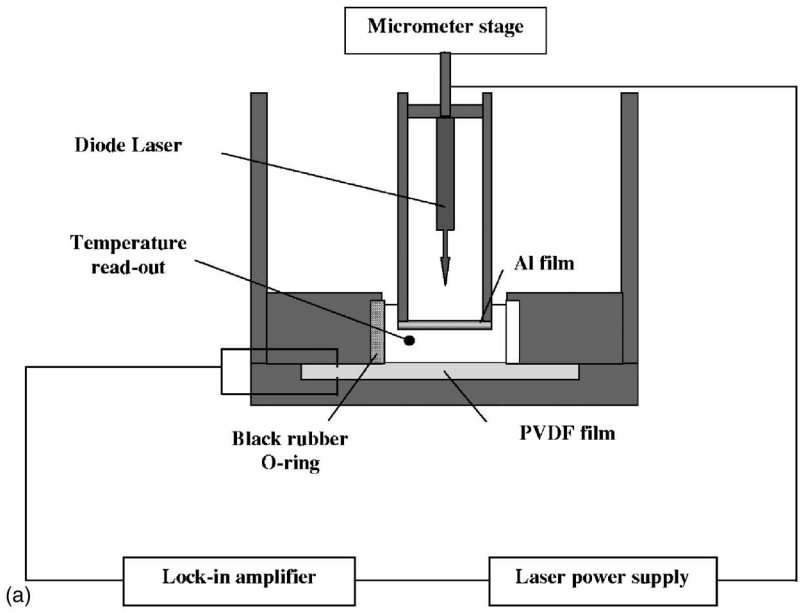

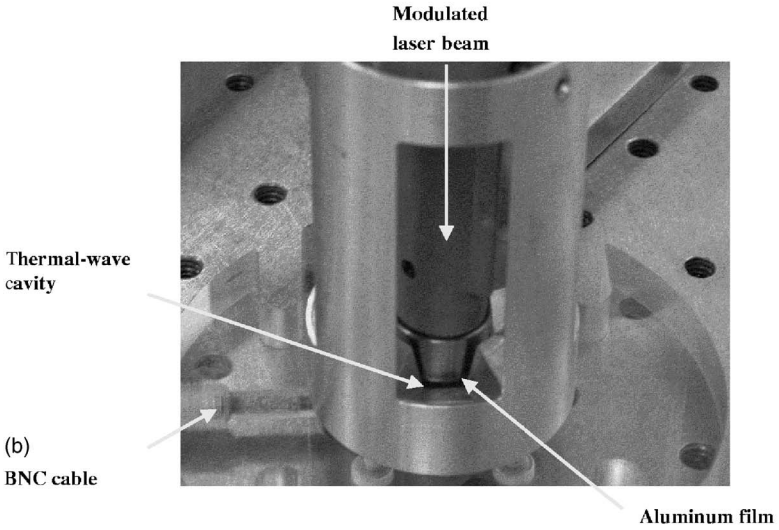

FIG. 1. Experimental setup: (a) schematic cross section; (b) actual sensor.

length. The main goal of the present study is to develop a three-dimensional theoretical model for the temperature field of the conventional thermal-wave cavity configuration applied in our recent studies[4,13] and its comparison to signals obtained using one-dimensional theory. Besides the intrinsic value of this comparison for precise TWRC thermophysical measurements, the present study can be very useful for determining conditions under which the considerably simpler one-dimensional (1D) theoretical models of intracavity thermal-wave fields can be safely used for these measurements.

II. THERMAL-WAVE CAVITY CONFIGURATION

A typical experimental TWRC setup[4,13] for liquids (Fig. 1) consists of the measurement cell, a diode laser (Coherent, $\lambda = 809.6$ nm), a laser controller (Coherent, model 6060), and a lock-in amplifier (Stanford Research Systems SR830).

The design of the measurement cell involves fixed dimensions of the cavity length for obtaining reproducible measurements with various types of liquid solutions. The laser beam was incident on the 106-μm-thick aluminum film which converted the modulated optical intensity to thermal waves propagating through the liquid sample. The intensity of the laser radiation was modulated using the internal oscillator of the lock-in amplifier. A pyroelectric film (Measurement Specialties, Inc., 52 μm-thick Ni–Al PVDF film) detected the temperature oscillations and produced the output signal measured by the lock-in amplifier.

III. ONE-DIMENSIONAL THEORETICAL APPROACH

The three-dimensional (3D) structure of the thermal-wave cavity is shown in Fig. 2(a). It includes four adjacent layers of symmetrical cylindrical geometry. The three-dimensional Gaussian laser beam of spot size W impinges on the aluminum film. The thermal-wave cavity scheme applied in one-dimensional theoretical analysis[4,13] is presented in Fig. 2(b). The cavity consists of four layers: aluminum film ($L_s = 0.106$ mm), water (or other liquid) layer ($L_w = 0.6$ mm), pyroelectric film, PVDF, ($L_p = 0.052$ mm), and aluminum

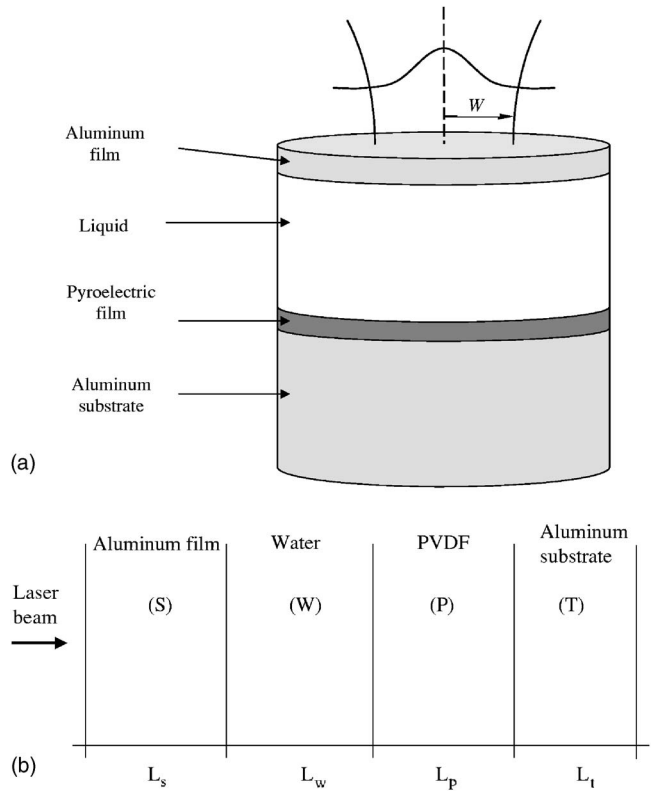

FIG. 2. Measurement cell: (a) Geometry of a cylindrical thermal-wave resonant cavity of finite radius irradiated by a Gaussian laser beam of spot size W; (b) one-dimensional scheme of the cavity.

backing support (L_t=5 mm). The thermal-wave equation for each layer of the system (Fig. 2) in the absence of a heat source can be written as

$$\frac{d^2}{dx^2}T_n(x,\omega) - \sigma_n^2 T_n(x,\omega) = 0,$$

$$\sigma_n = (1+i)\sqrt{\pi f/\alpha_n}, \tag{1}$$

where the parameter σ_n is the complex thermal-wave diffusion coefficient,[1] which includes the thermal diffusivity α_n of the nth layer. The detailed solution of Eq. (1) with appropriate boundary conditions for the cavity filled with a liquid sample is derived in our previous study.[4] In the developed one-dimensional four-layer theoretical model,[4] conduction and radiation heat transfer inside the cavity (liquid layer) were considered. However, in order to simplify the task of the present work, we will only consider the low-frequency range of frequency scans (Fig. 3), where the radiation component is negligible compared with conduction[4] and the three-dimensional character of the intracavity thermal-wave

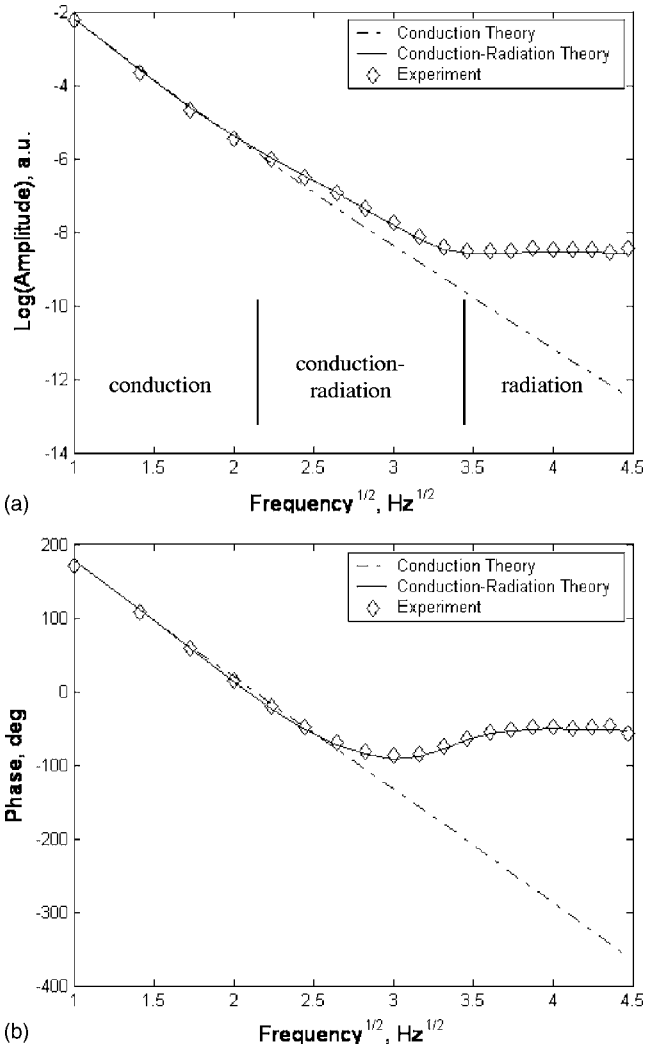

FIG. 3. Experimental and theoretical curves vs the square root of modulation frequency at the cavity length L=0.6 mm using water as sample: (a) amplitude; (b) phase.

field is most likely to manifest itself. The purely conductive frequency range for water-filled TWRC extends up to 4–5 Hz, as deduced from Figs. 3(a) and 3(b). Gas-filled cavities have not exhibited measurable radiation heat transfer.[4]

Taking into account the relation between the modulated temperature of the PVDF film and the measured signal:[3]

$$V(\omega) = S(\omega)\frac{1}{L_p}\int_{L_p} T_p(x,\omega)dx, \tag{2}$$

where $S(\omega)$ is an instrumental transfer function factor, the simplified (conduction only) expression for the PVDF signal[4] thus becomes

$$V(\omega) = \frac{S(\omega)(4I_0/k_p\sigma_p^2)e^{-L_s\sigma_s}e^{-L_w\sigma_w}(1-e^{-L_p\sigma_p})(Y_{tp}+X_{tp}e^{-L_p\sigma_p})}{b_{wp}P_{tp}Q_{sw}+Q_{tp}P_{sw}}, \tag{3}$$

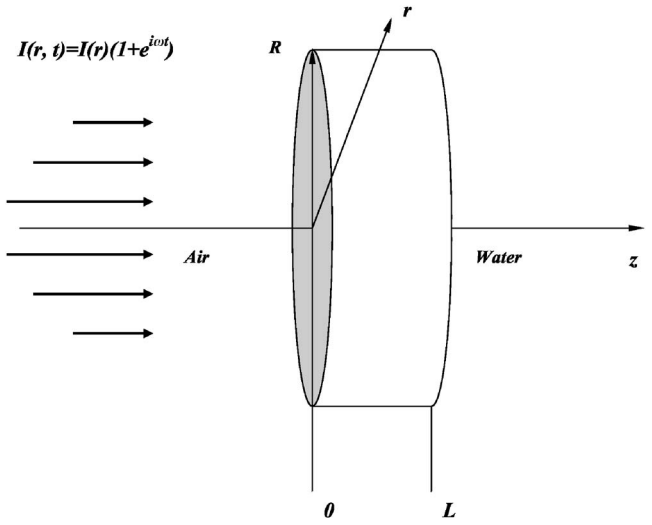

FIG. 4. Three-dimensional circular thermal-wave cavity wall impinged by a modulated Gaussian laser beam.

where I_0 is the laser intensity, σ_j was determined in Eq. (1), and

$$b_{ij} = \frac{k_i \sigma_i}{k_j \sigma_j},$$

$$X_{ij} = (1 - b_{ij}) + (1 + b_{ij}) e^{-2L_i \sigma_i},$$

$$Y_{ij} = (1 + b_{ij}) + (1 - b_{ij}) e^{-2L_i \sigma_i},$$

$$P_{ij} = (Y_{ij} + X_{ij} e^{-2L_j \sigma_j}),$$

$$Q_{ij} = (Y_{ij} - X_{ij} e^{-2L_j \sigma_j}). \quad (4)$$

The instrumental factor $S(\omega)$ can be experimentally normalized out[4,13] by taking the ratio of the cavity signal to the photopyroelectric signal produced by direct laser light incident on the PVDF sensor. The thermal diffusivity of liquids was obtained by fitting the theory to the ratio of the experimental data of the measured PVDF signals versus modulation frequency for these two configurations.

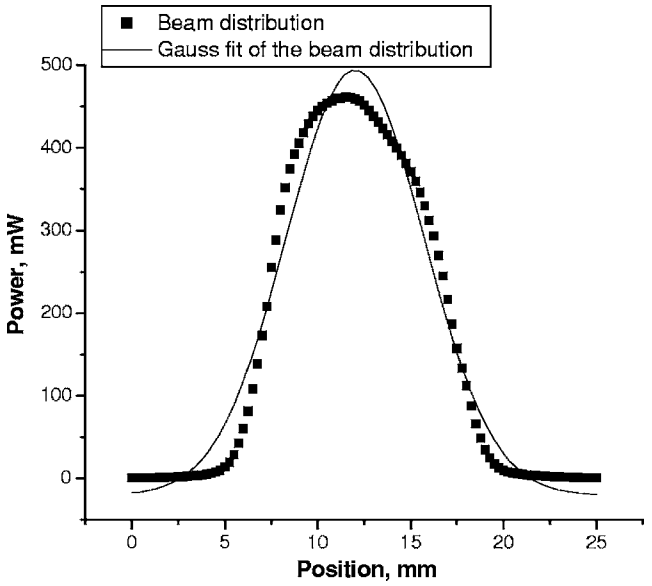

FIG. 5. Laser beam profile, $W=3.7$ mm.

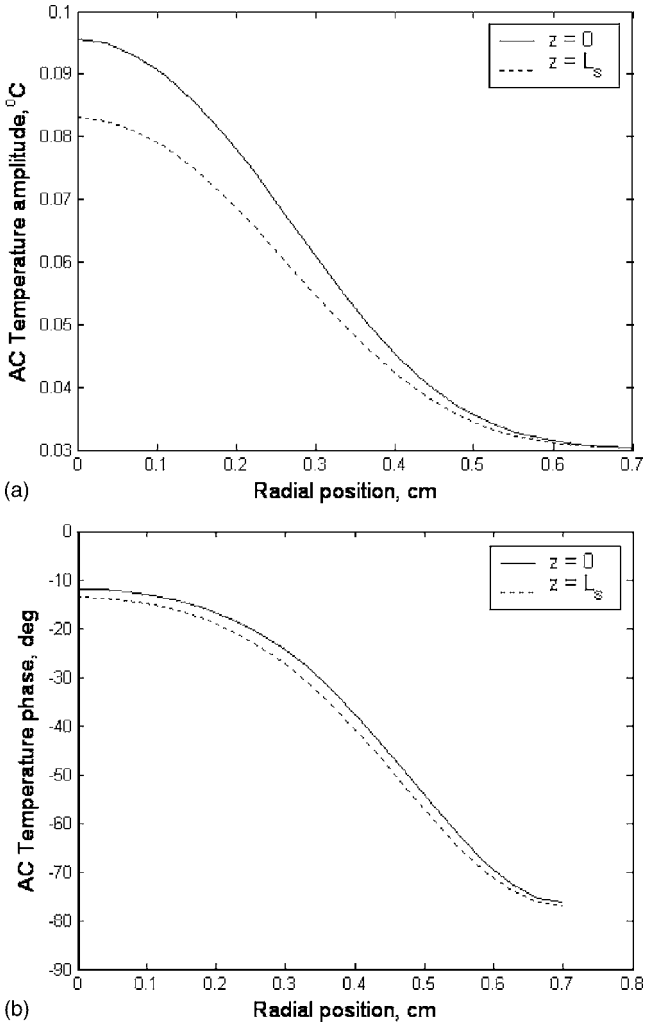

FIG. 6. 3D-temperature distribution in the aluminum film, with $k_s = 28$ W m^{-1} K^{-1}, $\alpha_s = 8.7 \times 10^{-5}$ m^2 s^{-1}, $k_a = 2.62 \times 10^{-2}$W m^{-1} K^{-1}, $\alpha_a = 2.18 \times 10^{-5}$ m^2 s^{-1}, $k_w = 0.603$ W m^{-1} K^{-1}, $\alpha_w = 1.43 \times 10^{-7}$ m^2 s^{-1}, $L_s = 0.106$ mm, $R=7$ mm, $W=3.7$ mm, Bi=0, and $f=3$ Hz: (a) amplitude, (b) phase.

IV. THREE-DIMENSIONAL MODEL

To verify the limits of validity of the one-dimensional approach in the practical case of a Gaussian laser beam profile, the one-dimensional and surface-area averaged three-dimensional temperature profiles were calculated and compared (conduction heat transfer only) with the experimental data. In order to simplify the solution of the three-dimensional problem, the four-layer system was solved layer by layer. Figure 4 describes a periodically modulated laser beam incident on a circular aluminum film bounded by air and water layers.

The laser beam is incident on the front surface of the film comprising the upper cavity wall. The beam profile for the semiconductor diode laser applied in the study (the beam radius is 3.7 mm) and its Gaussian fit are shown in Fig. 5. The relatively poor fit of the actual beam profile into a

Gaussian can be explained by the fact that semiconductor diode lasers usually do not exhibit ideal TEM_{00} Gaussian profiles.

The 3D thermal-wave distribution in an opaque sample is described by the thermal diffusion equation

$$\frac{\partial^2 T}{\partial r^2}+\frac{1}{r}\frac{\partial T}{\partial r}+\frac{\partial^2 T}{\partial z^2}=\frac{1}{\alpha}\frac{\partial T}{\partial t}-\frac{1}{2k}I(r)[1+\exp(i\omega t)],$$

$$T=T(r,z;\omega), \tag{5}$$

subject to the following boundary conditions:

$$-k_s\frac{\partial T}{\partial z}(r,0,\omega)=\frac{1}{2}I(r)[1+\exp(i\omega t)]-k_a\frac{\partial T}{\partial z}(r,0,\omega),$$

$$-k_s\frac{\partial T}{\partial z}(r,L,\omega)=-k_w\frac{\partial T}{\partial z}(r,L,\omega),$$

$$-k_s\frac{\partial T}{\partial r}(R,z,\omega)=hT(R,z,\omega), \tag{6}$$

where $I(r)=I_0\exp(-r^2/W^2)$. Here, α and k are the thermal diffusivity and the thermal conductivity, respectively, of the cylindrical sample. h is the heat transfer coefficient of the circumferential boundary of the cylindrical sample. The subscripts a, s, and w stand for air, aluminum film, and water, respectively. The solution can be conveniently obtained using a Green function approach. The 3D Green function equation for an isotropic material and source is [Ref. 1, Eq. (5.3)]

$$\frac{1}{r}\frac{\partial}{\partial r}\left[r\frac{\partial}{\partial r}G(r,z|r_0,z_0;\omega)\right]+\frac{\partial^2}{\partial z^2}G(r,z|r_0,z_0;\omega)-\sigma^2 G(r,z|r_0,z_0;\omega)=-\frac{1}{2\pi\alpha r}\delta(r-r_0)\delta(z-z_0), \tag{7}$$

where the time dependence $(1/2)(1+e^{i\omega t})$ is implied on both sides of the equation. The extension of the radial field is finite, so separation of variables gives

$$G(r,z|r_0,z_0;\omega)=F(r)Z(z),$$

$$\frac{\partial}{\partial r}\left(r\frac{\partial F}{\partial r}\right)+\lambda^2 rF=0,$$

$$\frac{\partial^2 Z}{\partial z^2}-\xi^2 Z=0,\quad \xi^2=\sigma^2+\lambda^2. \tag{8}$$

The general r-dependent solution bounded at $r=0$ is

$$F(r)=AJ_0(\lambda r), \tag{9}$$

where A and λ are constants to be determined and J_0 is the Bessel function of the first kind of order zero. Homogeneous boundary conditions of the third kind applied to the r-dependent equation yield

$$-k_s\frac{\partial}{\partial r}J_0(\lambda r)\big|_{r=R}=k_s\lambda J_1(\lambda R)=hJ_0(\lambda R), \tag{10}$$

leading to the following eigenvalue equation:

$$\alpha_n J_1(\alpha_n)-\left(\frac{hR}{k_s}\right)J_0(\alpha_n)=0,\quad \alpha_n=\lambda R. \tag{11}$$

In this work, the roots α_n were used as tabulated in the literature.[14]

Finally, Eq. (9) becomes

$$F_n(r)=A_nJ_0\left(\alpha_n\frac{r}{R}\right). \tag{12}$$

Now the Green function can be written in the following form:

$$G_<(r,z|r_0;\omega)=\sum_{n=1}^{\infty}J_0\left(\alpha_n\frac{r}{R}\right)[a_n\exp(-\xi_n z)+b_n\exp(\xi_n z)],\quad 0\leqslant z\leqslant z_0,$$

$$G_>(r,z|r_0;\omega)=\sum_{n=1}^{\infty}J_0\left(\alpha_n\frac{r}{R}\right)[c_n\exp(-\xi_n z)+d_n\exp(\xi_n z)],\quad z_0\leqslant z\leqslant L. \tag{13}$$

The continuity of the Green function and discontinuity of the derivative at $z=z_0$ (z_0 is location of the thermal harmonic impulse) gives

$$\frac{\partial}{\partial z}G_>(r,z|r_0;\omega)\big|_{z=z_0+\varepsilon}-\frac{\partial}{\partial z}G_<(r,z|r_0;\omega)\big|_{z=z_0-\varepsilon}=\frac{\delta(r-r_0)}{2\pi\alpha r}, \tag{14}$$

$$G_>(r,z_0+\varepsilon|r_0;\omega)=G_<(r,z_0-\varepsilon|r_0;\omega). \tag{15}$$

Owing to the third-kind boundary conditions at $r=R$, the Dirac delta function must be expanded as [Ref. 1, Eq. (5.74)]

$$\frac{\delta(r-r_0)}{r}=\frac{2}{R^2}\sum_{n=1}^{\infty}\frac{J_0[\alpha_n(r/R)]J_0[\alpha_n(r_0/R)]}{J_0^2(\alpha_n)+J_1^2(\alpha_n)}. \tag{16}$$

The boundary conditions at $z=0$, L are

$$k_s\left.\frac{\partial G(r,z|r_0;\omega)}{\partial z}\right|_{z=0}=k_a\left.\frac{\partial G(r,z|r_0;\omega)}{\partial z}\right|_{z=0},$$

$$k_s\left.\frac{\partial G(r,z|r_0;\omega)}{\partial z}\right|_{z=L}=k_w\left.\frac{\partial G(r,z|r_0;\omega)}{\partial z}\right|_{z=L}. \tag{17}$$

Finally, the Green function becomes

$$G(r,z|r_0;\omega)=\frac{1}{2\pi\alpha R^2}\sum_{n=1}^{\infty}\frac{J_0[\alpha_n(r/R)]J_0[\alpha_n(r_0/R)]}{\xi_n(J_0^2(\alpha_n)+J_1^2(\alpha_n))}$$
$$\times\begin{cases}\exp[-\xi_n(z-z_0)]+\gamma_{as}\gamma_{sw}\exp\{-\xi_n[2L-(z-z_0)]\}+\gamma_{as}\exp[-\xi_n(z+z_0)]+\gamma_{sw}\exp\{-\xi_n[2L-(z+z_0)]\}, & 0\leqslant z\leqslant z_0\\ \exp[-\xi_n(z_0-z)]+\gamma_{as}\gamma_{sw}\exp\{-\xi_n[2L-(z_0-z)]\}+\gamma_{as}\exp[-\xi_n(z+z_0)]+\gamma_{sw}\exp\{-\xi_n[2L-(z+z_0)]\}, & z_0\leqslant z\leqslant L.\end{cases} \tag{18}$$

The field equation in the presence of the planar Gaussian source is

$$T(r,z;\omega)=\frac{2\pi\alpha}{k_s}\int_0^R r_0dr_0\int_0^L Q(r_0;\omega)G(r,z|r_0,z_0;\omega)dz_0,$$

$$Q(r_0;\omega)=\frac{1}{2}I_0\exp\left(-\frac{r_0^2}{W^2}\right)[1+\exp(i\omega t)]. \tag{19}$$

Using the following definitions:

$$\xi_n^2=\frac{\alpha_n^2}{R^2}+i\frac{\omega}{\alpha},\quad b_{ij}=\frac{k_i\xi_i}{k_j\xi_j},\quad \gamma_{ij}=\frac{1-b_{ij}}{1+b_{ij}},$$

$$F_n(R,W)=\int_0^R\exp\left(-\frac{r_0^2}{W^2}\right)J_0\left(\alpha_n\frac{r_0}{R}\right)r_0dr_0, \tag{20}$$

the temperature field expression can be written as

$$T_s(r,z;\omega)=\frac{I_0}{2k_sR^2}\sum_{n=1}^{\infty}\frac{J_0[\alpha_n(r/R)]F_n(R,W)(1+\gamma_{as})\{\exp(-\xi_nz)+\gamma_{sw}\exp[-\xi_n(2L_s-z)]\}}{\xi_n[1+(\mathrm{Bi}/\alpha_n)^2]J_0^2(\alpha_n)[1-\gamma_{as}\gamma_{sw}\exp(-2\xi_nL_s)]}, \tag{21}$$

where $\mathrm{Bi}=hR/k_s$ is the Biot number. The integral F_n in the numerator has an analytical solution, however, in this work it was calculated numerically.

An estimate of the heat transfer coefficient equivalent between the aluminum film and the silicone sealant surrounding the film on the circumferential surface was performed according to Ref. 1, Lemma 2.1. This lemma states that in order to transform third-kind boundary conditions to the equivalent second-kind (adiabatic) boundary conditions in thermal-wave fields, the heat transfer coefficient h should be replaced by the product $k_j\sigma_j$, where j is the spatial region surrounding the heated material. This lemma can be used to considerably reduce the complexity of the coupled-layer thermal-wave field through the elimination of thermal coupling loss and its replacement by an equivalent heat loss factor. Estimates show that for the thermal effusivity of silicone[15] equal to 1.4 W m^{-2} K^{-1} s$^{1/2}$, the heat transfer coefficient equivalent, h, at 3 Hz equals 4.3 W m^{-2} K^{-1}, and the corresponding Biot number equals $\mathrm{Bi}=0.001\approx 0$. The calculation of the thermal-wave profile at the air ($z=0$) and water ($z=L_s$) boundaries of the aluminum film as a function of radial position r [Eq. (21)] for adiabatic boundary conditions at the circumference is presented in Fig. 6.

Due to the high conductivity and very small thickness of the aluminum film, the phase lag changes only slightly between $z=0$, where the laser beam impinges on the surface (air boundary), and $z=L_s$ (fluid/gas boundary of the film), so laser beam generated radial thermal-wave profile can be considered as approximately the same at both surfaces of the aluminum film with a small reduction in the amplitude. This assumption is important in order to apply the theoretical approach to the fluid layer in contact with the aluminum film. The presence of a thin metallic cavity wall renders any intracavity fluid a "pseudo-opaque" layer, i.e., a layer that has fluid (here water) thermophysical properties but infinite (surface) absorption coefficient. In this case, all light is absorbed and heat is generated right at the surface of the aluminum-water interface. Hence, the mathematical description of the temperature distribution in the water layer can be the same as derived for the aluminum layer [Eq. (21)] with the only change being that the boundary conditions must include water-aluminum and water-PVDF interfaces, instead of aluminum-air and aluminum-water interfaces considered for the aluminum film of Fig. 4. The resulting thermal-wave field in the intracavity region becomes

$$T_w(r,z;\omega)=\frac{I_0}{2k_wR^2}\sum_{n=1}^{\infty}\frac{J_0[\alpha_n(r/R)]F_n(R,W)(1+\gamma_{sw})\{\exp(-\xi_nz)+\gamma_{wp}\exp[-\xi_n(2L_w-z)]\}}{\xi_n[1+(\mathrm{Bi}/\alpha_n)^2]J_0^2(\alpha_n)[1-\gamma_{sw}\gamma_{wp}\exp(-2\xi_nL_w)]}, \tag{22}$$

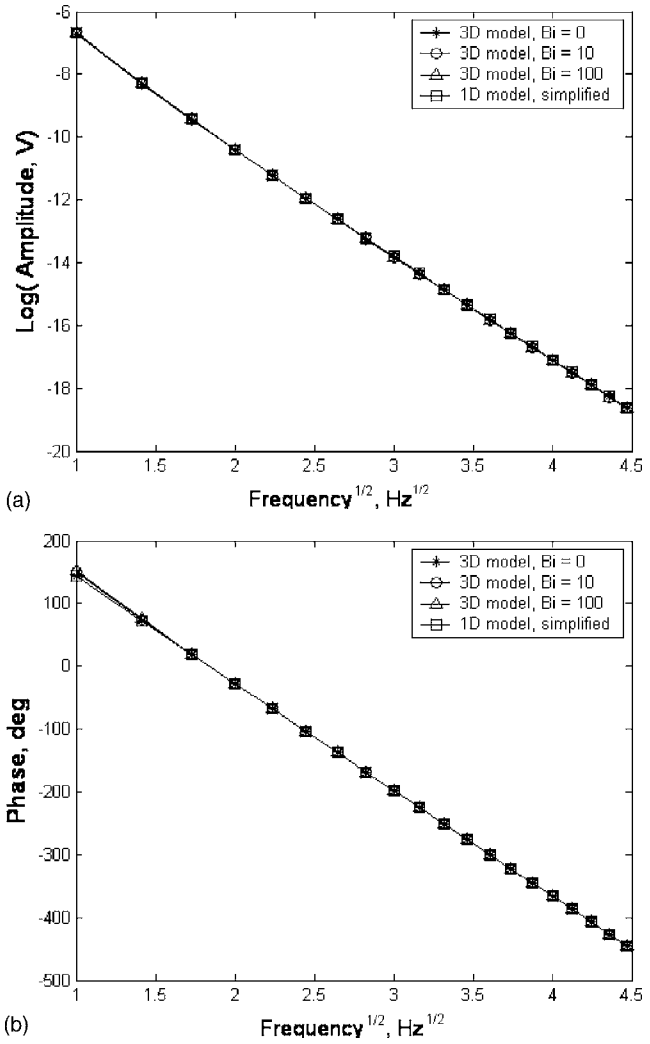

FIG. 7. Frequency dependence of the averaged signal calculated according to the 3D model [Eq. (24)], $W=3.7$ mm, and simplified 1D model [Eq. (26)]: (a) amplitude, (b) phase.

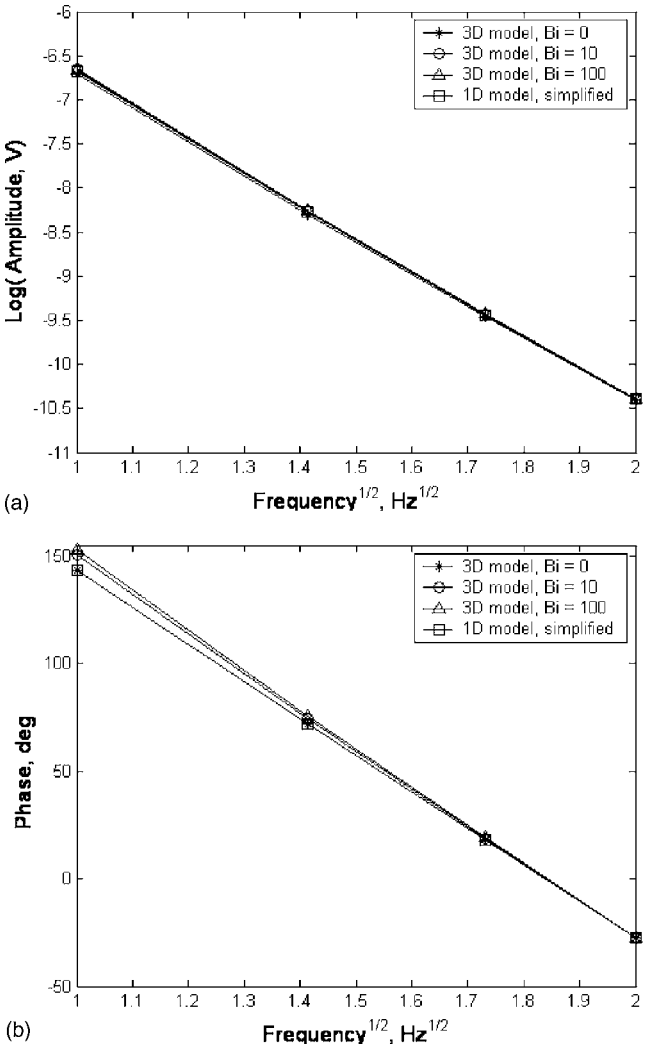

FIG. 8. Zoomed-in frequency dependence of the averaged signal calculated according to the 3D model [Eq. (24)], $W=3.7$ mm, and simplified 1D model [Eq. (26)] of Fig. 7 in the frequency range of 1–4 Hz: (a) amplitude, (b) phase.

where $\mathrm{Bi}=hR/k_w$.

The estimate of the heat transfer coefficient equivalent in the sense of Lemma 2.1 (Ref. 1) between water and black rubber ring surrounding the thermal-wave cavity on the circumferential surface of the water layer shows that for thermal effusivity of black rubber[16] equal to 1.2×10^3 W m^{-2} K^{-1} s$^{1/2}$, the Biot number equals $\mathrm{Bi}=33$. Finally, the temperature profile at the water-PVDF interface, $z=L_w$, can be averaged over the surface as

$$T_{\mathrm{av}}(L_w,\omega)=\frac{2\pi\int_0^R T_w(r,L_w;\omega)rdr}{\pi R^2}. \tag{23}$$

Here $R=0.7$ cm is the radius of the cavity cell and $T_w(r,L_w;\omega)$ is calculated from Eq. (22). Then, for thermally thick pyroelectric elements, the signal averaged over the PVDF film thickness can be obtained according to the exponential decay law:

$$V_{\mathrm{3D}}=\frac{1}{L_p}\int_0^{L_p} T_{\mathrm{av}}(L_w,\omega)\exp(-\sigma_p z)dz, \tag{24}$$

where L_p is the thickness of the PVDF film. In this manner, the experimentally measured signal, which is actually the averaged output of the pyroelectric sensor (i.e., PVDF film), can be compared with the (3D) theoretical calculations.

V. 1D AND 3D MODEL COMPARISONS AND EXPERIMENT

To compare the calculated 3D profile [Eq. (24)] with the 1D four-layer model [Eq. (3)], the 1D calculations were performed for simplified conditions similar to those used in the 3D formalism, namely, $L_s=0$, $L_p\to\infty$, and $L_t=0$ [Fig. 2(b)]. The 1D equation (3) then reduces to

$$V_{\mathrm{1D}}(\omega)=\frac{S(\omega)(4I_0/k_p\sigma_p^2)e^{-L_w\sigma_w}Y_{tp}}{b_{wp}P_{tp}Q_{sw}+Q_{tp}P_{sw}}, \tag{25}$$

and, using Eq. (4), it further reduces to

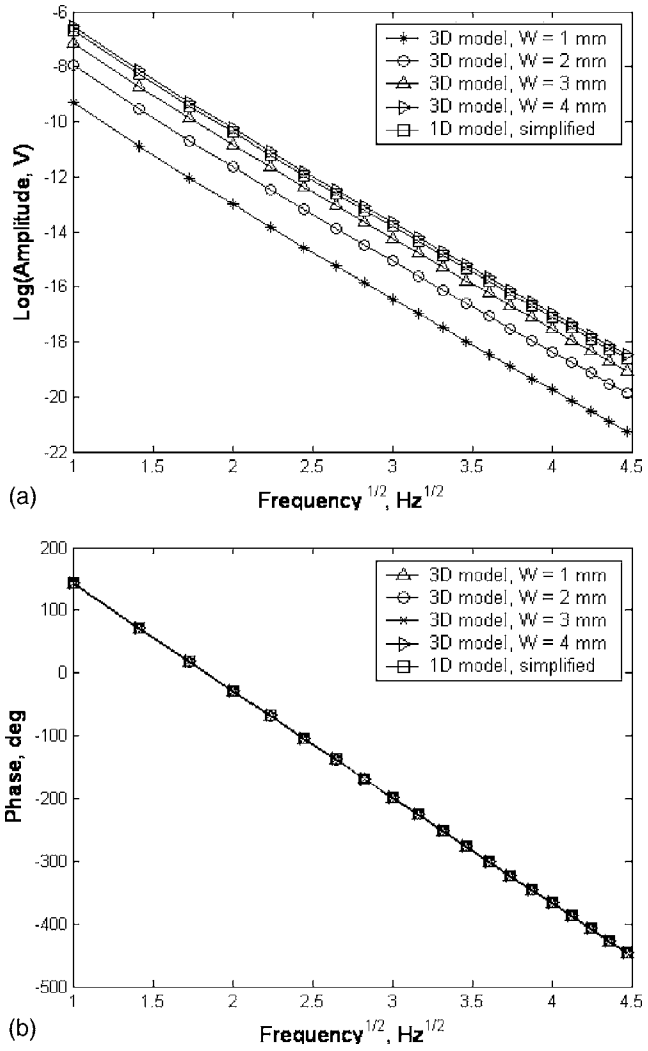

FIG. 9. Frequency dependence of the averaged signal calculated according to 3D model [Eq. (24)] and simplified 1D model [Eq. (26)] with various beam sizes and Bi=0: (a) amplitude; (b) phase.

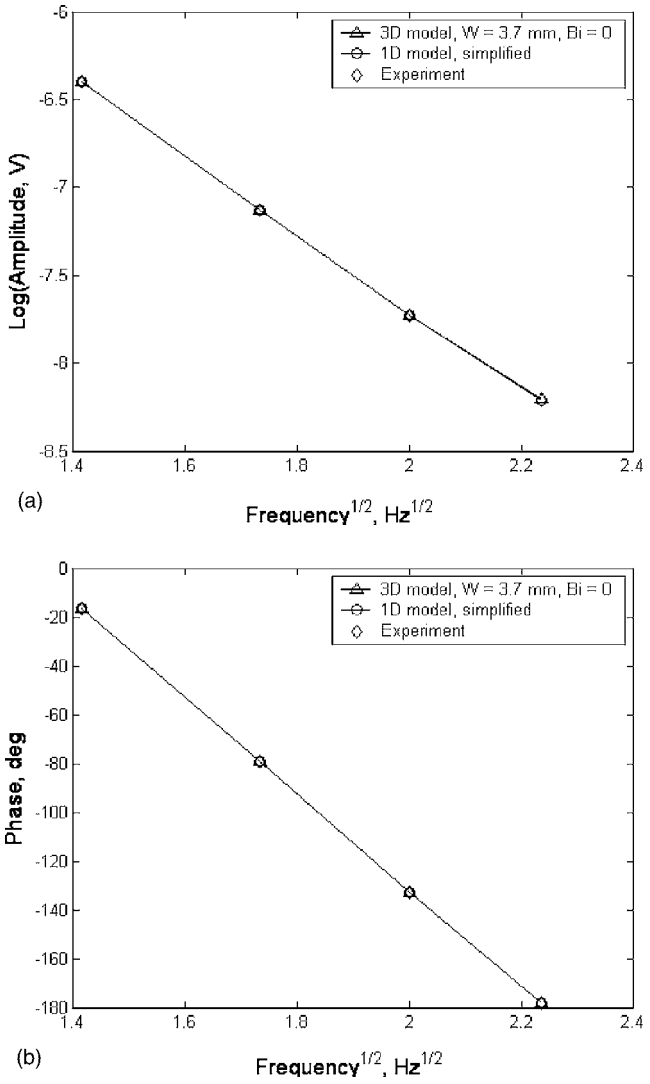

FIG. 10. Comparison of the simplified 1D and 3D theoretical frequency dependencies to the experimental data: (a) amplitude, (b) phase.

$$V_{1D}(\omega) = \frac{S(\omega)(2I_0/k_p\sigma_p^2)e^{-L_w\sigma_w}}{(1+b_{wp})(1+\gamma_{wp}e^{-2L_w\sigma_w})}. \quad (26)$$

The instrumental transfer function $S(\omega)$ was found using the experimental data and the 1D four-layer model [Eq. (3)].

The comparison revealed the influence of two main parameters which can cause the three dimensionality of the problem, namely, W and Bi. The results of simulations are presented in Figs. 7 and 8–9. Figures 7 and 8 show the frequency dependence of the three-dimensional profile [Eq. (24)] at the water-PVDF interface averaged over the PVDF thickness for several Biot numbers and $W=3.7$ mm. It is seen that three-dimensional effects should be taken into account for Biot numbers up to 100 when the frequency is less than 2–3 Hz. In our study, the frequency range involved in the fitting of thermal diffusivity values was usually 2–12 Hz. According to these calculations, the temperature field in this range is not affected by the circumferential heat transfer for Biot numbers less than 100. As was mentioned above, the Biot number for our experimental conditions is Bi=33, so one can assume Bi=0 to further simplify the analysis. The influence of the beam size on the dimensionality of the problem is demonstrated in Fig. 9. This figure shows no phase dependence on the beam size for the conditions of the experiment throughout the scanned frequency range, while the amplitude obviously grows with intensity I_0 held constant due to the increased laser beam size and the subsequent optical power delivery to the aluminum overlayer, in agreement with the exponential dependence of the function F_n on beam size W [Eq. (20)]. However, this dependence does not influence the dimensionality of the field as witnessed by the constancy of amplitude slopes and phase values.

The signal amplitude and phase calculated according to the simplified 1D [Eq. (26)] and 3D [Eq. (24)] models are presented in Fig. 10 and compared with the experimental data for pure water. The results clearly justify the one dimensionality of the problem for the conditions of the study.

In conclusion, the one dimensionality of the TWRC field cannot be justified *a priori*. This study has shown that, in order to use one-dimensional TWRC theory for thermal property fits, one must ensure that the influence on the thermal-wave distribution of lateral (radial) heat transfer through the cavity boundaries is appropriately estimated, and

the beam size of the laser light used in the experiments is large enough, in order to keep the thermal-wave field within the one-dimensional formalism, thus greatly simplifying and strengthening the quantitative importance of TWRCs as thermophysical property sensor device.

ACKNOWLEDGMENT

The support of the National Sciences and Engineering Research Council of Canada (NSERC) is gratefully acknowledged.

[1] A. Mandelis, *Diffusion-Wave Fields: Mathematical Methods and Green Functions* (Springer-Verlag, New York, 2001), p. 87.
[2] *Principles and Perspectives of Photothermal and Photoacoustic Phenomena*, edited by A. Mandelis (North-Holland, New York, 1991), and references therein.
[3] A. Mandelis and M. Zver, J. Appl. Phys. **57**, 4421 (1985).
[4] A. Matvienko and A. Mandelis, Int. J. Thermophys. **26**, 837 (2005).
[5] J. A. Balderas-Lopez, A. Mandelis, and J. A. Garcia, Rev. Sci. Instrum. **71**, 2933 (2000).
[6] D. Dadarlat, C. Neamtu, E. Surducan, A. H. Sahraoui, S. Longuemart, and D. Bicanic, Instrum. Sci. Technol. **30**, 387 (2002).
[7] M. Chirtoc, E. H. Bentefour, C. Glorieux, and J. Thoen, Thermochim. Acta **377**, 105 (2001).
[8] D. Dadarlat, J. Gibkes, D. Bicanic, and A. Pasca, J. Food. Eng. **30**, 155 (1996).
[9] J. Shen and A. Mandelis, Rev. Sci. Instrum. **66**, 4999 (1995).
[10] J. A. P. Lima, M. G. da Silva, M. S. Sthel, S. L. Cardoso, and H. Vargas, Rev. Sci. Instrum. **74**, 433 (2003).
[11] C. Wang and A. Mandelis, Rev. Sci. Instrum. **70**, 2372 (1999).
[12] A. Mandelis, J. Vanniasinkam, S. Budhudu, A. Othonos, and M. Kokta, Phys. Rev. B **48**, 6808 (1993).
[13] A. Matvienko and A. Mandelis, Rev. Sci. Instrum. **76**, 1 (2005).
[14] J. V. Beck, K. D. Cole, A. Haji-Sheikh, and B. Litkouhi, *Heat Conduction Using Green's Functions* (Hemisphere, Washington, 1992).
[15] T. Bhowmick, B. R. Gupta, and S. Pattanayak, Cryogenics **32**, 623 (1992).
[16] C. Hu, J. H. Zhao, and J. Shen, Rev. Sci. Instrum. **74**, 459 (2003).